Electrochemistry from First Principles in the Grand Canonical Ensemble

Arihant Bhandari,[†,‡] Chao Peng,[¶,‡] Jacek Dziedzic,[†,§,‡] Lucian Anton,[‖] John R. Owen,[†,‡] Denis Kramer,[¶,‡,⊥] and Chris-Kriton Skylaris[*,†,‡]

[†]*School of Chemistry, University of Southampton, Highfield, Southampton SO17 1BJ, United Kingdom*

[‡]*The Faraday Institution, Quad One, Becquerel Avenue, Harwell Campus, Didcot, OX11 0RA, United Kingdom*

[¶]*Engineering Sciences, University of Southampton, Southampton SO17 1BJ, United Kingdom*

[§]*Faculty of Applied Physics and Mathematics, Gdansk University of Technology, Gdansk 80-233, Poland*

[‖]*Atos UK*

[⊥] *Helmut-Schmidt-University, University of the Armed Forces, 22043 Hamburg, Germany*

E-mail: C.Skylaris@soton.ac.uk

Abstract

Progress in electrochemical technologies such as automotive batteries, supercapacitors and fuel cells depends greatly on developing improved charged interfaces between electrodes and electrolytes. The rational development of such interfaces can benefit from the atomistic understanding of the materials involved by first principles quantum mechanical simulations with Density Functional Theory (DFT). However, such

simulations are typically performed on the electrode surface in the absence of its electrolyte environment and at constant charge. We have developed a new hybrid computational method combining DFT and the Poisson-Boltzmann equation (P-BE) capable of simulating experimental electrochemistry under potential control, in the presence of solvent and electrolyte. The charged electrode is represented quantum-mechanically via linear-scaling DFT which can model nanoscale systems with thousands of atoms and is neutralized by a counter electrolyte charge via the solution of a modified P-BE. Our approach works with the total free energy of the combined multiscale system in a grand canonical ensemble of electrons subject to a constant electrochemical potential. It is calibrated with respect to the reduction potential of common reference electrodes such as the standard hydrogen electrode and the Li-metal electrode, which is used as a reference electrode in Li-ion batteries. Our new method can be used to predict electrochemical properties under constant potential and we demonstrate this in exemplar simulations of the differential capacitance of few-layer graphene electrodes and the charging of a graphene electrode coupled to a Li metal electrode at different voltages.

1 Introduction

Progress in energy storage and conversion critically depends upon the understanding of electrochemical phenomena at the atomic level, particularly the charged nature of the electrode-electrolyte interface (EEI).[1–3] While the atomistic modelling of material systems from first principles has taken a leap with the development of density functional theory (DFT) which describes the nature of solid electrodes quite well,[4,5] an atomistic description of the charged EEI is still a big challenge because of the uncertainty in description of the electrolyte.[6]

One of the approaches for dealing with an electrolyte solution is via explicit solvation,[7–12] where there is an atomistic description of the solvent and electrolyte molecules on an equal footing as the main electrode. These methods require averaging over all degrees of freedom of solvent and electrolyte molecules, which is often computationally intractable. On the other

hand, hybrid quantum-continuum models are computationally efficient as they average out all the degrees of the surrounding electrolyte solution, while retaining an atomistic description of the explicit electrode system.[13,14] One can have the best of both methods by including adsorbed ions explicitly on the electrode surface treating these as a part of the quantum system, while treating the rest of the solution as implicit.

Several hybrid models of the EEI have been developed with a quantum-mechanical description for electrode and a continuum description of the solvent and electrolyte ions.[14–16] These models are generally controlled by the amount of charge on the solid electrode which imposes a constraint on the number of electrons and electrolyte ions in a canonical ensemble. However, charge transfer (both ions and electrons) between subsystems is a key process in electrochemical phenomena which is usually controlled by the applied voltage. This requires an open system of electrons and electrolyte ions under the influence of an applied voltage. It follows that the description of the electronic structure and electrolyte ions for a subsystem of an electrochemical model requires a formulation in the grand canonical ensemble. Such a subsystem of an electrochemical setup is shown in Fig. 1 schematically.

There are several important features of this subsystem: (1) it is periodic; (2) The electrolyte charge in the subsystem is not fixed as it varies to neutralize the surface charge on the electrode; (3) the number of electrons in the system are not fixed as they change under the constraint of a fixed electrochemical potential $\tilde{\mu}_{\mathrm{e}}$. In our previous papers, we have developed a hybrid quantum-continuum model with features (1),[16] and (2).[17] Now, we extend this model to include the third feature, which involves development of a method for DFT for electrons in a grand canonical ensemble at fixed electrochemical potential. This new development gives a complete computational framework for simulating electrochemical systems from first principles.

Kohn-Sham DFT[18] in the grand canonical ensemble is described in the book by Parr and Young.[19] Recent implementations in electrochemistry applications include that by Sundararaman *et al.* in the context of joint density functional theory,[20] by Melander *et al.* in

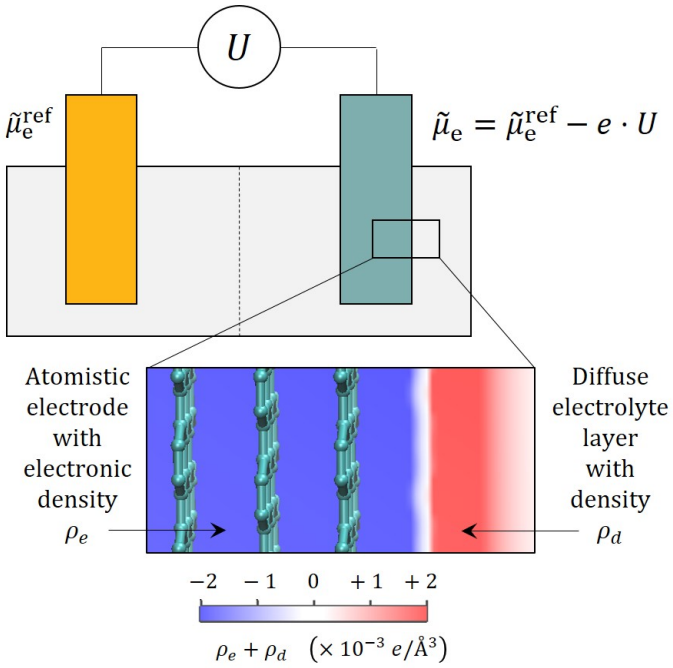

Figure 1: Subsystem of an electrochemical setup with a grand canonical ensemble for electrons and electrolyte ions under the control of an applied voltage U with respect to a reference electrode. Here, $\tilde{\mu}_e$ and $\tilde{\mu}_e^{ref}$ are the electrochemical potentials of electrons in the working and reference electrodes respectively.

the GPAW code,[21] by Hormann *et al.* in Quantum-ESPRESSO,[22] by Dufils *et al.* in the context of the finite field method.[11] Here, we develop a model for DFT for electrons in a grand canonical ensemble at a constant electrochemical potential in the ONETEP linear-scaling DFT code[23] whose computational cost scales linearly with the number of atoms as compared to the cubic-scaling in conventional DFT. This allows for quantum mechanical simulations with thousands of atoms therefore enabling computational exploration of complex atomistic models of electrode-electrolyte interfaces. Along with the implicit solvent and electrolyte model in ONETEP,[16,17,24,25] the newly-developed grand canonical method is a step towards a computational platform for large-scale *ab initio* electrochemistry controlled via an applied potential in an electrolyte environment as in experiments.

The application of the model is demonstrated on few-layer graphene based electrodes. Graphene based electrodes have been widely used in energy storage applications such as charge storage in supercapacitors, conductive additives in Li-ion batteries, etc.[26,27] Graphene

based supercapacitors can store charge in the electrode-electrolyte interface where the differential capacitance has been found to be promising experimentally.[28–33] Theoretical models have also tried to predict the differential capacitance of graphene based electrodes from first principles.[34–39] These theoretical simulations of the differential capacitance are based on the canonical ensemble approach, in which the charge on the electrode is fixed and the potential is calculated *a posteriori* from the difference in the electrostatic potential far away and the Fermi level of the electrons in the system. In this study, we apply our newly-developed grand canonical approach to simulations at controlled electrode potentials, and determine the differential capacitance self-consistently. This resembles the situation in experiments, where the voltage is controlled rather than the charge on the electrode.

To enable simulations of a general electrode system at fixed voltages with respect to any reference electrode, we calibrate the model parameters according to the absolute reduction potential of the standard hydrogen electrode (SHE),[40–42] and also that of the Li metal (Li^+/Li) electrode which is commonly used as the reference electrode in Li-ion batteries.[43]

During ultra short current spikes in a Li-ion battery, the charge storage at the interface also becomes important in addition to the Li-ion intercalation. We finally use our method to study this process by coupling a few-layer graphene electrode to the Li metal electrode at different voltages and examining the charge storage at the interface.

The outline of the paper is as follows: in the next sections, we describe the theory of our new method followed by an exemplar application on differential capacitance of few-layer graphene electrodes in supercapacitors. Thereafter, we describe the calibration of model parameters. Finally, we demonstrate a simulation of interfacial charge stored while connecting a graphene based electrode to Li metal electrode in a battery.

2 Theory

2.1 System

Our system includes an electrode embedded within a solvent and electrolyte ions. Out of the many possible ways of describing an electrochemical electrode in multi-scale modelling approaches,[44] in our model the electrode is treated quantum-mechanically via DFT, while the solvent is described as a dielectric continuum and the electrolyte is described as a diffuse layer of point-like mobile ions. This implicit treatment of the solvent and electrolyte ions is captured by the Poisson-Boltzmann equation.[45,46] The charge densities due to the two subsystems overlap in an interfacial region and interact not only via mean-field electrostatics but also have cavitation, dispersion and repulsion interactions. The total charge density $\rho_{\mathrm{t}}(\mathbf{r})$ can be written as the sum of that due to the quantum subsystem $\rho_{\mathrm{q}}(\mathbf{r})$ and the diffuse layer of electrolyte ions $\rho_{\mathrm{d}}(\mathbf{r})$. The quantum charge density consists of the charge density of electrons $\rho_{\mathrm{e}}(\mathbf{r})$ and the nuclear cores $\rho_{\mathrm{nuc}}(\mathbf{r})$, while the diffuse layer of electrolyte ions consists of charges $\{z_i\}$ with space-dependent concentrations $\{c_i(\mathbf{r})\}$, $i = 1 \dots p$:

$$\rho_{\mathrm{t}}(\mathbf{r}) = \rho_{\mathrm{q}}(\mathbf{r}) + \rho_{\mathrm{d}}(\mathbf{r})\,, \tag{1}$$

$$\rho_{\mathrm{q}}(\mathbf{r}) = \rho_{\mathrm{e}}(\mathbf{r}) + \rho_{\mathrm{nuc}}(\mathbf{r})\,, \tag{2}$$

$$\rho_{\mathrm{d}}(\mathbf{r}) = \sum_{i=1}^{p} z_i c_i(\mathbf{r})\,. \tag{3}$$

2.2 Free energy functional

Typical implementations of DFT are in systems with a constant number of electrons, also called a canonical ensemble of electrons. In such cases, the thermodynamic potential, the Helmholtz free energy is minimized, subject to a constraint on the number of electrons. while in electrochemistry applications, the number of electrons can change subject to a fixed electrochemical potential. This situation is described by a grand canonical ensemble

of electrons. In a grand canonical ensemble, the thermodynamic potential is a Legendre transform of the Helmholtz free energy, called the grand potential or the grand free energy. In such a situation the grand potential is minimized, subject to a constant electrochemical potential of electrons. In our model, the total free energy functional includes the grand potential of electrons Ω_{e}, the mean-field electrostatic functional Ω_{mf} and non-mean-field interactions Ω_{nmf}.

$$\Omega\left[\rho_{\mathrm{e}}, c_i, \nu\right] = \Omega_{\mathrm{e}}\left[\rho_{\mathrm{e}}\right] + \Omega_{\mathrm{mf}}\left[\rho_{\mathrm{e}}, c_i, \nu\right] + \Omega_{\mathrm{nmf}}\left[\rho_{\mathrm{e}}\right]. \tag{4}$$

The mean-field electrostatic functional Ω_{mf} is described in detail in our previous papers on the electrolyte model (Refs. 16,17). For the sake of completeness, we concisely summarize all the terms included in Ω_{mf} here:

$$\Omega_{\mathrm{mf}} = \frac{1}{2}\int_V \left[\rho_{\mathrm{e}}(\mathbf{r}) + \rho_{\mathrm{nuc}}(\mathbf{r}) + \rho_{\mathrm{d}}(\mathbf{r})\right]\nu(\mathbf{r})\,\mathrm{d}\mathbf{r} \quad \text{total electrostatic energy} \tag{5}$$

$$-\frac{1}{\beta}\sum_{i=1}^{p}\int_V c_i(\mathbf{r})\,\mathrm{d}\mathbf{r} \quad \text{electrolyte osmotic pressure} \tag{6}$$

$$-\frac{1}{\beta}\sum_{i=1}^{p}\int_V c_i(\mathbf{r})\ln\lambda(\mathbf{r})\mathrm{d}\mathbf{r} \quad \text{electrolyte accessibility repulsion energy} \tag{7}$$

$$+\frac{1}{\beta}\sum_{i=1}^{p}\int_V c_i(\mathbf{r})\ln\left(\frac{c_i(\mathbf{r})}{c^{\circ}}\right)\mathrm{d}\mathbf{r} \quad \text{electrolyte entropy term} \tag{8}$$

$$-\sum_{i=1}^{p}\mu_i\int_V c_i(\mathbf{r})\,\mathrm{d}\mathbf{r} \quad \text{electrolyte chemical potential term,} \tag{9}$$

where $\beta = \frac{1}{k_{\mathrm{B}}\theta}$, k_{B} is the Boltzmann constant, θ is the temperature, $\lambda(\mathbf{r})$ is the electrolyte accessibility function, c° is the standard thermodynamic reference of 1 mol/L (or 1 M) and μ_i are the chemical potentials of the electrolyte ions. Ω_{nmf} incorporates the non-mean-field interactions of cavitation, dispersion and repulsion with the continuum solvent, and is taken to be proportional to the solvent accessible surface area, where the proportionality constant

is a scaled surface tension of the solvent.[24,25] Minimization of the free energy functional with respect to the electrolyte concentrations $c_i(\mathbf{r})$ and the total electrostatic potential $\nu(\mathbf{r})$ gives the Poisson-Boltzmann equation:

$$\nabla \cdot (\varepsilon(\mathbf{r})\, \nabla \nu(\mathbf{r})) = -4\pi \left[\rho_{\mathrm{e}}(\mathbf{r}) + \rho_{\mathrm{nuc}}(\mathbf{r}) + \sum_{i=1}^{p} z_i c_i(\mathbf{r}) \right] \tag{10}$$

$$c_i(\mathbf{r}) = c_i^{\infty} \lambda(\mathbf{r}) \exp\{-\beta z_i \nu(\mathbf{r}) + \beta \mu_i^{\mathrm{ex}}\},\ i = 1 \ldots p$$

The solvent permittivity function $\varepsilon(\mathbf{r})$ is described as a smooth function: $\varepsilon(\mathbf{r}) = 1 + (\varepsilon^{\infty} - 1)\, \gamma(\mathbf{r})$, which varies from that in the bulk solvent ε^{∞} to 1 near the quantum region. We have implemented two choices for the interface function $\gamma(\mathbf{r})$: one following the Fattebert and Gygi function,[24,47] and the other one following the soft-sphere model of Fisicaro *et al.*[48,49] The electrolyte accessibility function $\lambda(\mathbf{r})$ is a smooth function varying from 1 in the bulk solution to 0 near the quantum system, which is represented as a similar product of overlapping spheres.[16] The concentration of electrolyte species 'i' far away in the bulk of the solution is c_i^{∞}. The Poisson-Boltzmann equation is solved using DL_MG,[50,51] a bespoke highly-parallel, multigrid, Poisson-Boltzmann solver library. The excess chemical potentials of the electrolyte ions μ_i^{ex} are determined to ensure electroneutrality of the total charge in periodic boundary conditions (PBCs) using the neutralization by electrolyte concentration shift (NECS) model described in our previous paper.[17] To handle the representation of point charges on a Cartesian grid, the nuclear cores are represented by smeared Gaussians (sg):

$$\rho_{\mathrm{nuc}}(\mathbf{r}) = \rho_{\mathrm{sg}}(\mathbf{r}) = \sum_{i}^{\mathrm{N}} \frac{Z_i}{(\alpha_i \sqrt{\pi})^3} e^{-\left(\frac{|\mathbf{r}-\mathbf{R}_i|}{\alpha_i}\right)^2}, \tag{11}$$

where N is the total number of atoms in the system. A smearing width (α_i) of $0.8\, a_0$ is used based on a previous parameter study.[25] The effect of this modification is corrected out in the energy expression (cf. eq. 14).

The grand potential of electrons Ω_{e} in eq. (4) is the Legendre transform of the Helmholtz

free energy A which converts the finite temperature canonical ensemble to the finite temperature grand canonical ensemble.[19]

$$\Omega_{\mathrm{e}}\left[\rho_{\mathrm{e}}\right] = A\left[\rho_{\mathrm{e}}\right] - \mu_{\mathrm{e}} \cdot N_{\mathrm{e}}, \tag{12}$$

where μ_{e} is the chemical potential of electrons and N_{e} is the number of electrons. A Helmholtz free energy functional can be defined as:

$$A\left[\rho_{\mathrm{e}}\right] = T_{\mathrm{s}}\left[\rho_{\mathrm{e}}\right] - \theta S_{\mathrm{s}}\left[\rho_{\mathrm{e}}\right] + E_{\mathrm{xc}}\left[\rho_{\mathrm{e}}\right] + V_{\mathrm{ps,nl}}\left[\rho_{\mathrm{e}}\right] \tag{13}$$

$$+ V_{\mathrm{ps,l}}\left[\rho_{\mathrm{e}}\right] - V_{\mathrm{sg-e}}\left[\rho_{\mathrm{e}}\right] + V_{\mathrm{ps-ps}} - V_{\mathrm{sg-sg}} \tag{14}$$

where T_{s} is the kinetic energy of non-interacting electrons, θ is the temperature, S_{s} is the entropy of non-interacting electrons, E_{xc} is the exchange-correlation energy functional, which is approximated in DFT, V_{ps} is the interaction energy with the pseudo-potential cores where the subscripts 'l' and 'nl' represent the local pseudopotential and the non-local part of the pseudopotential. In eq. (14), we replace the interaction energy of smeared Gaussians with electrons by that due to the local component of the pseudopotential, and also replace the interaction between smeared Gaussians with that between pseudopotential cores. These corrections in open and periodic boundary conditions are summarized in Table 1 of Ref. 16.

The electronic density ρ_{e} in Kohn-Sham DFT is constructed from the non-interacting orthonormal orbitals $\{\psi_i\}$ and their fractional occupancies $\{f_i\}$:

$$\rho_{\mathrm{e}}(\mathbf{r}) = \sum_i f_i \psi_i^*(\mathbf{r})\, \psi_i(\mathbf{r}) \tag{15}$$

The method thus becomes variational in terms of the orbitals $\{\psi_i\}$ and their occupancies $\{f_i\}$. The total number of electrons can be obtained from integrating the electronic density

over the entire volume of the simulation cell.

$$N_{\mathrm{e}} = \int_V \rho_{\mathrm{e}}(\mathbf{r})\,\mathrm{d}\mathbf{r} = \sum_i f_i. \tag{16}$$

The kinetic energy of non-interacting electrons in eq. (13) is:

$$T_{\mathrm{s}}\left[\rho_{\mathrm{e}}\right] \equiv T_{\mathrm{s}}\left[\{\psi_i\},\{f_i\}\right] = \sum_i f_i \int_V \psi_i^*(\mathbf{r}) \left(-\frac{1}{2}\nabla^2\right) \psi_i(\mathbf{r})\,\mathrm{d}\mathbf{r}, \tag{17}$$

and their entropy is:

$$S_{\mathrm{s}}\left[\rho_{\mathrm{e}}\right] \equiv S_{\mathrm{s}}\left[\{f_i\}\right] = -k_{\mathrm{B}} \sum_i \left[f_i \ln f_i + (1-f_i)\ln\left(1-f_i\right)\right], \tag{18}$$

where k_{B} is the Boltzmann constant. Similarly, the contribution due to the pseudopotentials can be written as:

$$\begin{aligned} V_{\mathrm{ps}}\left[\rho_{\mathrm{e}}\right] = V_{\mathrm{ps,nl}}\left[\rho_{\mathrm{e}}\right] + V_{\mathrm{ps,l}}\left[\rho_{\mathrm{e}}\right] &\equiv V_{\mathrm{ps,nl}}\left[\{\psi_i\},\{f_i\}\right] + V_{\mathrm{ps,l}}\left[\{\psi_i\},\{f_i\}\right] \\ &= \sum_i f_i \int_V \left|\psi_i(\mathbf{r})\right|^2 \left[\nu_{\mathrm{ps,nl}}(\mathbf{r}) + \nu_{\mathrm{ps,l}}(\mathbf{r})\right] \mathrm{d}\mathbf{r} \end{aligned} \tag{19}$$

Minimizing the total grand functional with respect to the orbitals $\{\psi_i\}$ gives the Kohn-Sham equations in the grand canonical ensemble:

$$\left[-\frac{1}{2}\nabla^2 + \nu_{\mathrm{eff}}\right] \psi_i = \epsilon_i \psi_i \tag{20}$$

where $\nu_{\mathrm{eff}} = \nu + (\nu_{\mathrm{ps,nl}} + \nu_{\mathrm{ps,l}} - \nu_{\mathrm{sg}}) + \delta E_{\mathrm{xc}}/\delta\rho_{\mathrm{e}}$. Here we have corrected the potential due to smeared Gaussians (sg) by the local component of the potential due to pseudopotential cores (ps). Minimizing the total grand free energy functional with respect to the orbital occupancies f_i gives:

$$k_{\mathrm{B}}\theta\left[\ln f_i - \ln\left(1-f_i\right)\right] + \epsilon_i - \mu_{\mathrm{e}} = 0, \tag{21}$$

which on rearranging, gives the Fermi-Dirac statistics:

$$f_i = \frac{1}{1 + \exp\{\beta\,(\epsilon_i - \mu_\mathrm{e})\}}. \tag{22}$$

Solving the Kohn-Sham eigenvlaue problem in eq. (20) subject to orthonormality of orbitals $\{\psi_i\}$ is an $\mathcal{O}(N^3)$ procedure. The cubic-scaling computational cost puts a restriction on the size of systems that can be studied with DFT, typically up to a few hundred atoms. ~~While~~ However, modelling of complex problems requires large-scale systems with sizes extending to thousands of atoms. This has motivated development of $\mathcal{O}(N)$ approaches,[52] such as ONETEP.

2.3 ONETEP

ONETEP is a linear-scaling DFT program, where the conventional DFT has been reformulated in terms of the single-particle density matrix so that the computational cost scales linearly with the number of atoms.[23,53] In ONETEP, we use non-orthogonal generalized Wannier functions (NGWFs),[54] expanded in a basis set of periodic sinc functions,[55] which are equivalent to a plane wave basis set. The NGWFs $\{\phi_\alpha\}$ are notionally related to the orthonormal Kohn-Sham orbitals via a linear transformation $\phi_\alpha(\mathbf{r}) = \sum_i \psi_i(\mathbf{r})\, M_{i\alpha}$, or $\psi_i(\mathbf{r}) = \phi_\alpha(\mathbf{r})\, M_i^\alpha$. Here and henceforth, we use implicit summation over repeated Greek indices. Within this representation the electronic density can be written as $\rho_\mathrm{e}(\mathbf{r}) = \phi_\alpha(\mathbf{r})\, K^{\alpha\beta} \phi^*_\beta(\mathbf{r})$, where $\{K^{\alpha\beta}\}$ are the elements of the density kernel matrix $K^{\alpha\beta} = \sum_i M_i^\alpha f_i M_i^{\dagger\beta}$. Using this formalism in eq. (13), the kinetic energy can be written as $T_\mathrm{s}[\rho_\mathrm{e}] \equiv T_\mathrm{s}[\{\psi_i\},\{f_i\}] \equiv T_\mathrm{s}[\{\phi_\alpha\},\mathbf{K}] = K^{\alpha\beta} \left\langle \phi_\beta \left| -\frac{1}{2}\nabla^2 \right| \phi_\alpha \right\rangle$, and the contribution due to the pseudopotentials can be written as: $V_\mathrm{ps}[\rho_\mathrm{e}] \equiv V_\mathrm{ps}[\{\phi_\alpha\},\mathbf{K}] = K^{\alpha\beta} \left\langle \phi_\beta \left| \nu_\mathrm{ps} \right| \phi_\alpha \right\rangle = K^{\alpha\beta} \left\langle \phi_\beta \left| \nu_\mathrm{ps,l} \right| \phi_\alpha \right\rangle + K^{\alpha\beta} \left\langle \phi_\beta \left| \nu_\mathrm{ps,nl} \right| \phi_\alpha \right\rangle$, where the subscripts 'l' and 'nl' represent the local pseudopotential and the non-local part of the pseudopotential in the Kleinman and Bylander representation. Similarly, the first term in eq. (5) can be written as: $1/2 \cdot \int \rho_\mathrm{e}(\mathbf{r})\, \nu(\mathbf{r})\, \mathrm{d}\mathbf{r} = 1/2 \cdot K^{\alpha\beta} \left\langle \phi_\beta \left| \nu \right| \phi_\alpha \right\rangle$. Instead of solving

the Kohn-Sham eigenvalue problem in eq.(20) directly, in ONETEP the ground state is calculated using direct minimization of total free energy and a linear-scaling computational cost is achieved due to the localization of NGWFs and the truncation of the density kernel. The algorithm for minimization of the total grand potential in the grand canonical ensemble for electrons is implemented within the finite temperature ensemble DFT (EDFT) functionality of ONETEP.[56]

2.4 Finite temperature ensemble DFT in ONETEP

Here, we briefly review the finite temperature ensemble DFT approach in ONETEP which was originally developed in a canonical ensemble of electrons.[56] In the canonical ensemble, the Helmholtz free energy A is minimized directly in nested loops. The outer loop optimizes the NGWFs $\{\phi_\alpha\}$ by minimizing a projected Helmholtz free energy functional:

$$A'\left[\{\phi_\alpha\}\right] \equiv \min_{\{H_{\alpha\beta}\}} \Omega\left[\{H_{\alpha\beta}\}, \{\phi_\alpha\}\right] \tag{23}$$

with respect to the NGWFs, where $\{H_{\alpha\beta}\}$ are the elements of the Hamiltonian matrix, $H_{\alpha\beta} = \left\langle \phi_\alpha \middle| \hat{H} \middle| \phi_\beta \right\rangle$. The derivative of the projected Helmholtz free energy with respect to the NGWFs can be written as:

$$\left|\Gamma^\beta\right\rangle = \frac{\delta A'}{\delta \left\langle \phi_\beta \right|} = \hat{H} \left|\phi_\gamma\right\rangle K^{\gamma\beta}. \tag{24}$$

Applying orthonormality by projecting out the component of the derivative parallel to the NGWFs, we get the following expression for the NGWF gradient in the cannical ensemble:

$$\begin{aligned} |\tilde{\Gamma^\beta}\rangle &= \left|\Gamma^\beta\right\rangle - \left|\phi_\eta\right\rangle S^{\eta\sigma} \left\langle \phi_\sigma \middle| \Gamma^\beta \right\rangle \\ &= \hat{H} \left|\phi_\gamma\right\rangle K^{\gamma\beta} - \left|\phi_\eta\right\rangle S^{\eta\sigma} H_{\sigma\gamma} K^{\gamma\beta}, \end{aligned} \tag{25}$$

where $\{S_{\alpha\beta}\}$ are the elements of the overlap matrix $S_{\alpha\beta} = \langle\phi_\alpha|\phi_\beta\rangle$. The total Helmholtz free energy is minimized until the NGWF gradient is below a threshold. The inner loop involves a diagonalization of the Hamiltonian matrix as

$$H_{\alpha\beta}M_i^\beta = S_{\alpha\beta}M_i^\beta\epsilon_i. \tag{26}$$

Although, the diagonalization procedure is cubic-scaling, the use of localized minimal basis set of NGWFs ensures that the size of Hamiltonian matrix and the prefactor due to diagonalization is minimal, thereby reducing the computational cost. From the obtained eigenvalues ϵ_i the chemical potential of electrons (Fermi level) μ_e is calculated subject to the constraint on the number of electrons:

$$\sum_i f_i = \sum_i \frac{1}{1+\exp\{\beta\left(\epsilon_i - \mu_\mathrm{e}\right)\}} = N_e. \tag{27}$$

At every inner loop iteration the Hamiltonian matrix is updated and the Helmholtz free energy $A\left[\{H_{\alpha\beta}\},\{\phi_\alpha\}\right]$ is minimized subject to constant NGWFs $\{\phi_\alpha\}$. The minimization converges when the commutator $[H_{\alpha\beta}, K_{\alpha\beta}]$ and the change in Fermi level μ_e is below a threshold. All throughout, a self-consistent direct minimization approach is used, which ensures convergence towards the Kohn-Sham ground-state at every step and completely removes charge sloshing effects.[57] Now, we describe the newly-developed approach for electrons in a grand canonical ensemble.

2.5 The ~~new~~ grand canonical algorithm

In the grand canonical ensemble of electrons, instead of the Helmholtz free energy A, the grand potential Ω (and Ω_e) in eq. 4 (and 12) is directly minimized in nested loops subject to a constant Fermi level and no constraint on the number of electrons. The outer loop

optimizes the NGWFs $\{\phi_\alpha\}$ by minimizing a projected grand functional:

$$\Omega' \left[\{\phi_\alpha\}\right] \equiv \min_{\{H_{\alpha\beta}\}} \Omega \left[\{H_{\alpha\beta}\}, \{\phi_\alpha\}\right] \tag{28}$$

with respect to the NGWFs The derivative of the projected grand free energy with respect to the NGWFs can be written as:

$$\begin{aligned} \left|\Gamma^\beta\right\rangle = \frac{\delta\Omega'}{\delta \left\langle\phi_\beta\right|} &= \frac{\delta A'}{\delta \left\langle\phi_\beta\right|} - \mu_\mathrm{e} \frac{\delta \mathrm{tr}(\mathbf{KS})}{\delta \left\langle\phi_\beta\right|} \\ &= \hat{H} \left|\phi_\gamma\right\rangle K^{\gamma\beta} - \mu_\mathrm{e} \left|\phi_\gamma\right\rangle K^{\gamma\beta} \end{aligned} \tag{29}$$

Applying orthonormality by projecting out the component of the derivative parallel to the NGWF, we get:

$$\begin{aligned} \left|\tilde{\Gamma^\beta}\right\rangle &= \left|\Gamma^\beta\right\rangle - \left|\phi_\eta\right\rangle S^{\eta\sigma} \left\langle\phi_\sigma\middle|\Gamma^\beta\right\rangle \\ &= \hat{H} \left|\phi_\gamma\right\rangle K^{\gamma\beta} - \mu_\mathrm{e} \left|\phi_\gamma\right\rangle K^{\gamma\beta} - \left|\phi_\eta\right\rangle S^{\eta\sigma} H_{\sigma\gamma} K^{\gamma\beta} + \mu_\mathrm{e} \left|\phi_\eta\right\rangle K^{\eta\beta} \\ &= \hat{H} \left|\phi_\gamma\right\rangle K^{\gamma\beta} - \left|\phi_\eta\right\rangle S^{\eta\sigma} H_{\sigma\gamma} K^{\gamma\beta}, \end{aligned} \tag{30}$$

which is the same as the NGWF gradient for the canonical ensemble (cf. eq. (25)). The term containing the chemical potential μ_e cancels out in eq. (30), therefore the gradient of the grand functional with respect to the NGWFs is independent of the chemical potential of electrons μ_e. The total grand potential is minimized until the NGWF gradient is below a threshold. The inner loop also follows a similar procedure to the canonical ensemble involving the diagonalization of the Hamiltonian matrix. In the canonical ensemble, the chemical potential of electrons μ_e is determined from the eigenvalues to satisfy the constraint on the number of electrons as in eq. (27), whereas in grand canonical ensemble the chemical potential of electrons μ_e is constant, rather the number of electrons and the charge on the

system is determined as:

$$N_{\mathrm{e}} = \sum_i f_i = \sum_i \frac{1}{1 + \exp\{\beta\,(\epsilon_i - \mu_{\mathrm{e}})\}}, \tag{31}$$

$$q = Z_{\mathrm{ion}} - e \cdot N_{\mathrm{e}}, \tag{32}$$

where Z_{ion} is the charge on the nuclear cores. At every inner loop iteration the Hamiltonian matrix is updated and the grand free energy $\Omega\left[\{H_{\alpha\beta}\}, \{\phi_\alpha\}\right]$ is minimized subject to constant NGWFs $\{\phi_\alpha\}$. The minimization converges when the commutator $[H_{\alpha\beta}, K_{\alpha\beta}]$ and the change in the number of electrons N_{e} is below a threshold. Thus the algorithms for the canonical and grand canonical EDFT approaches are very similar with the difference being in the constraints on the system (constant number of electrons in the canonical ensemble versus constant chemical potential in the grand canonical ensemble) and the relevant thermodynamic potential (free energy) being minimized (Helmholtz free energy in the canonical ensemble versus grand free energy in the grand canonical ensemble). The control over chemical potential in the grand canonical ensemble allows for simulations at controlled voltages as in electrochemical applications.

2.6 Connection with electrochemistry

In typical situations in electrochemistry, the electrochemical potential of electrons in an electrode is controlled with respect to a reference electrode. The electrochemical potential is defined as:[1,2]

$$\tilde{\mu}_{\mathrm{e}} = \mu_{\mathrm{e}} - e \cdot \Phi, \tag{33}$$

where μ_{e} is the chemical potential of electrons, e is the elementary charge ($1.602176634 \times 10^{-19}$ coulombs or 1.0 in atomic units) and Φ is the macroscopic electrostatic potential or the electrostatic potential far away in the electrolyte solution, $\Phi = \nu(\mathbf{r} \to \infty)$.[40] The electrostatic potential far away is zero in any solution of the Poisson-Boltzmann equation,[16,17,42] which is

also discussed in Sec. 3.1.1. Hence, in our model the electrochemical potential is the same as the chemical potential of electrons ($\tilde{\mu}_{\mathrm{e}} = \mu_{\mathrm{e}}$) and by controlling the chemical potential of electrons one can simulate the situation in electrochemistry experiments. This is similar to the formulation in Ref. 40. The chemical potential of electrons (or the Fermi level) can be set with respect to a reference electrode:

$$\mu_{\mathrm{e}} = \mu_{\mathrm{e}}^{\mathrm{ref}} - e \cdot U, \tag{34}$$

where $\mu_{\mathrm{e}}^{\mathrm{ref}}$ is the chemical potential of electrons in the reference electrode and U is the potential of the working electrode with respect to the reference electrode. On controlling the potential U to the set point, electronic current passes through the external circuit from the working electrode to the reference electrode or vice-versa adjusting μ_{e} until the condition of eq. (34) is satisfied. A rapid electronic equilibration, due to a high electron mobility, is useful in supercapacitors and also in a battery cell over very short times.

In Sec. 3.2, we calibrate our model parameters to set the chemical potential of the reference electrode to that of the standard hydrogen electrode on the absolute scale $\mu_{\mathrm{e}}^{\mathrm{SHE}} \equiv \mu_{\mathrm{e}}^{\mathrm{H^+/H_2}} = -4.44$ eV.[58] We also calibrate model parameters according to the absolute potential of Li metal electrode, $\mu_{\mathrm{e}}^{\mathrm{Li^+/Li}} = -1.39$ eV (3.05 eV with respect to SHE)[58] which is useful for applications in simulations of Li-ion battery electrodes.[43] The values of electronic energies ($\mu_{\mathrm{e}}^{\mathrm{ref}}$) as well as reduction potentials ($\mathcal{E}$) on the absolute scale and relative to SHE, from Ref. 58 are given in Table 1. We note here that the convention of electronic energies ($\mu_{\mathrm{e}}^{\mathrm{ref}}$) which is used inside typical electronic structure packages is opposite in sign to the electrostatic scale (Φ, U and $\mathcal{E}$) due to the negative charge on the electron.

Table 1: The electrochemical potentials in different scales (Ref. 58)

System	$\mathcal{E}$, relative to SHE (V)	$\mathcal{E}$, absolute scale (V)	$\mu_{\mathrm{e}}^{\mathrm{ref}}$, physical scale (eV)
Electron in vac.	-4.44	0.0	0.0
Li^+/Li	-3.05	1.39	-1.39
H^+/H_2 (SHE)	0.0	4.44	-4.44

2.7 Differential capacitance

The charge storage at an electrode-electrolyte interface can be quantified in terms of the differential capacitance. In a canonical approach, the charge q is fixed as an input and then the electrode potential U is computed, while in the grand canonical ensemble, the electrode potential U is fixed and the charge q is determined. The differential capacitance is defined as the slope of the charge versus potential curve:

$$C = \frac{d\sigma}{dU}, \tag{35}$$

where $\sigma = q/A$ is the charge per unit surface area of the electrode. The total capacitance of the electrode and electrolyte can be considered as two capacitances in series:

$$\frac{1}{C_{\mathrm{t}}} = \frac{1}{C_{\mathrm{electrolyte}}} + \frac{1}{C_{\mathrm{electrode}}} \tag{36}$$

For metallic electrodes, the capacitance due to the electrode side is so high so that the total capacitance, is limited by the electrolyte side alone. While for semi-conductor or semi-metal electrodes, both the capacitances are of the same order of magnitude. As the electrode charge develops in the electronic density of states and in our model, the electrolyte is a diffuse layer of electrolyte ions, so we simplify the notation as:

$$\frac{1}{C_{\mathrm{t}}} = \frac{1}{C_{\mathrm{d}}} + \frac{1}{C_{\mathrm{e}}}, \tag{37}$$

Now we describe some results from our model which include an exemplar application on calculating the differential capacitance of graphene based electrodes in supercapacitors, calibration of model parameters according to the reduction potential of standard hydrogen electrode (SHE) and Li metal electrode, followed by a demonstration of the model on the interfacial charge storage during ultra fast charging in Li-ion batteries.

3 Results and Discussion

3.1 Exemplar application on differential capacitace of graphene based electrodes

In the following subsections, we discuss the electrolyte diffuse layer capacitance, the electronic capacitance and the total capacitance of few-layer graphene based electrodes respectively.

3.1.1 Electrolyte diffuse layer capacitance (C_{d})

The electrolyte in our model is represented as a diffuse layer of Poisson-Boltzmann electrolyte. The charge developed in the diffuse layer of the electrolyte is equal and opposite (in sign) to the charge developed on the graphene electrode in order to achieve electroneutrality resembling a situation in a supercapacitor. The charge versus potential curves can be computed naturally with a grand canonical DFT approach as the one developed in this paper. We also compare and validate our results with those from a canonical ensemble approach. We perform simulations of 1-5 layer AB-stacked graphene electrodes with 96 C atoms in each layer placed in the middle of a simulation cell of dimensions $17.08\text{Å} \times 14.80\text{Å} \times 90.42\text{Å}$. The aqueous solution is represented as a Poisson-Boltzmann electrolyte of bulk concentration $c_i^{\infty} = 6$ M in an implicit solvent with a bulk permittivity of 78.54 and surface tension of 0.07415 N/m, same as that of water at 298.15 K. While the surface tension can itself change with the electrolyte concentration,[59] it is taken to be same as that for the pure water. We use the density based model for the solvent permittivity function with previously benchmarked parameters.[24] For the electrolyte accessibility function we use a density isovalue of 0.001 e/a_0^3 and a solvent radius of 3.0 a_0 based on previous calibration tests.[16] The ~~psinc~~ kinetic energy cutoff for periodic sinc functions is 1000.0 eV and the NGWF radius is 8.0 a_0 (4.23 Å) for C atoms.

In the canonical ensemble we fix the charge on the system q and obtain the electrode potential *a posteriori*. We take the neutral system ($q = 0$) as the reference. The change in

the planar average electrostatic potential ($\Delta\nu$) with respect to a neutral system ($q = 0$) for different values of charge q in the canonical ensemble ($\Delta\nu(q) = \nu(q) - \nu(q = 0)$) is plotted in Fig. 2(a) for two sample values of q for single layer graphene. The electrostatic potential away from the graphene layer is zero and does not change with the state of charge of the system. As a result, the electrode potential U with respect to the potential of zero charge (pzc) can be determined as simply the change in the chemical potential of electrons:

$$-e \cdot U(q) = \mu_{\mathrm{e}}(q) - \mu_{\mathrm{e}}(q = 0). \tag{38}$$

In the grand canonical ensemble, we do the reverse, we fix the electrode potential *a priori* and thereby the chemical potential of electrons:

$$\mu_{\mathrm{e}}(U) = \mu_{\mathrm{e}}^{\mathrm{ref}} - e \cdot U. \tag{39}$$

Here, the Fermi level of the neutral system has been taken as the reference ($\mu_{\mathrm{e}}^{\mathrm{ref}} = \mu_{\mathrm{e}}^{q=0}$). The change in the planar average electrostatic potential ($\Delta\nu$) with respect to the pzc ($U = 0$) is plotted for two different values of the electrode potential U in the grand canonical ensemble ($\Delta\nu(U) = \nu(U) - \nu(U = 0)$) in Fig. 2(b). The electrostatic potential away from the graphene layer is zero and does not change with the state of charge of the system. The charge on the system is obtained *a posteriori* from eq. (32).

Now we show the convergence behaviour for the calculations of single layer graphene in electrolyte solution. In ONETEP, these calculations in electrolyte solution are started from a calculation which has converged first in vacuum. The convergence of chemical potential (Fermi level) of electrons μ_e with the number of EDFT inner loop iterations in the canonical ensemble is shown in Fig. 3(a) for different values of charge on the system q. The convergence threshold on the change in Fermi level $\Delta\mu_e$ is 10^{-6} eV. The convergence of the charge q with the number of EDFT inner loop iterations in the grand canonical ensemble is shown in Fig. 3(b). The convergence threshold for the change in the number of electrons ΔN_{e} is 10^{-4} for

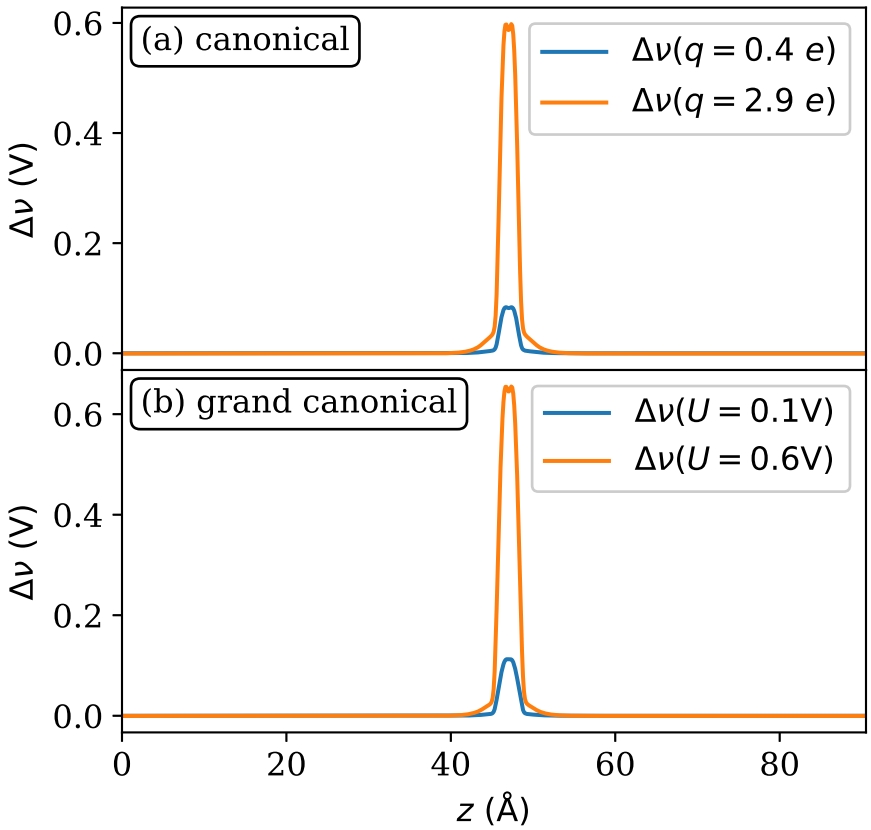

Figure 2: Change in the planar average electrostatic potential profile ($\Delta\nu$) around a single layer graphene in 6 M aqueous electrolyte solution, (a) with respect to the neutral system ($\Delta\nu(q) = \nu(q) - \nu(q = 0)$) for two different values of charge q in the canonical ensemble, and (b) with respect to the potential of zero charge charge ($\Delta\nu(U) = \nu(U) - \nu(U = 0)$) for two different values of the electrode potential U in the grand canonical ensemble.

the entire system ($= 10^{-6}$ per atom). The convergence is reached easily in few NGWF outer loop iterations (less than 6), comprising of several inner loop EDFT iterations (maximum 10 per outer loop).

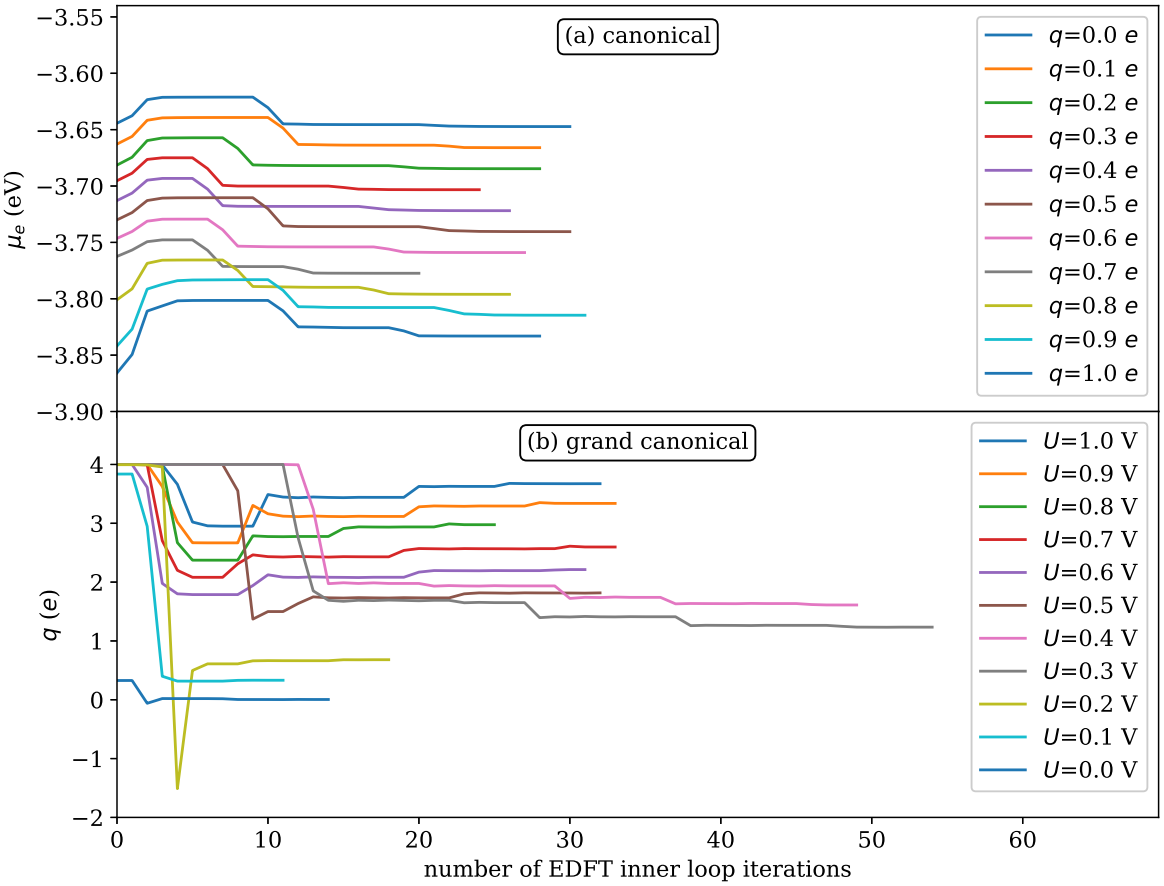

Figure 3: Convergence of ~~the~~ (a) chemical potential (Fermi level) of electrons μ_e at different values of charge on the system q in the canonical ensemble and (b) charge on the system q at different values of electrode potential U in the grand canonical ensemble; with respect to the number of iterations ~~in grand canonical ensemble~~ in inner loop of ensemble DFT (~~GC-~~EDFT) ~~at different values of electrode potential U~~.

The corresponding charge density $\sigma_{\mathrm{d}} = q/A$ versus the electrode potential U curves for the canonical and grand canonical ensembles are shown in Fig. 4 for single-layer graphene. For the canonical ensemble we scan the charge at a step of $\Delta q = 0.1\ e$ and for the grand

canonical ensemble, we scan the potential at a step of $\Delta U = 0.1$ V. As can be seen, the grand canonical results are quite similar to the results from the canonical ensemble. The variation of surface charge with electrode potential is quite linear as also observed in previous computational studies.[34,36,37]

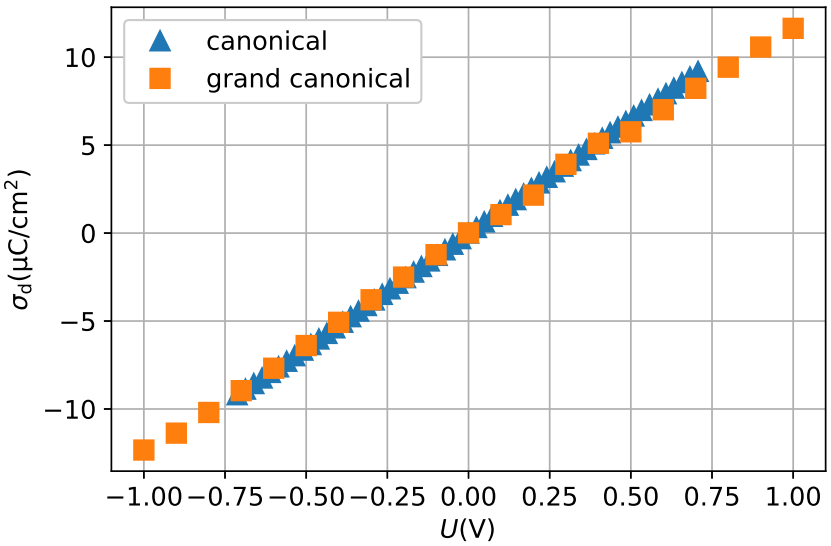

Figure 4: Charge density σ_d versus the electrode potential U for a single layer graphene in the canonical and grand canonical ensemble for electrons.

The planar-average electrolyte concentration profiles around positively charged single layer graphene are shown in Fig. 5 for two example cases of a canonical ensemble at $q = 2.9\ e$ and a grand canonical ensemble at $U = 0.7$ V. As the graphene layer is positively charged in both cases, there is a build up of negatively charged electrolyte ions around the graphene layer and a depletion of positively charged electrolyte ions to neutralize the overall charge. The asymptotic concentration goes to the bulk value of 6 M and the double layer is created at the interface.

After validating our grand-canonical method with the canonical ensemble for single layer graphene, we now repeat the potential-charge experiment in the grand canonical ensemble for 1-5 layer graphene showing the results in Fig. 6. The charge density σ_d is quite linear with the potential and the electrolyte diffuse layer capacitance C_d is calculated as the slope

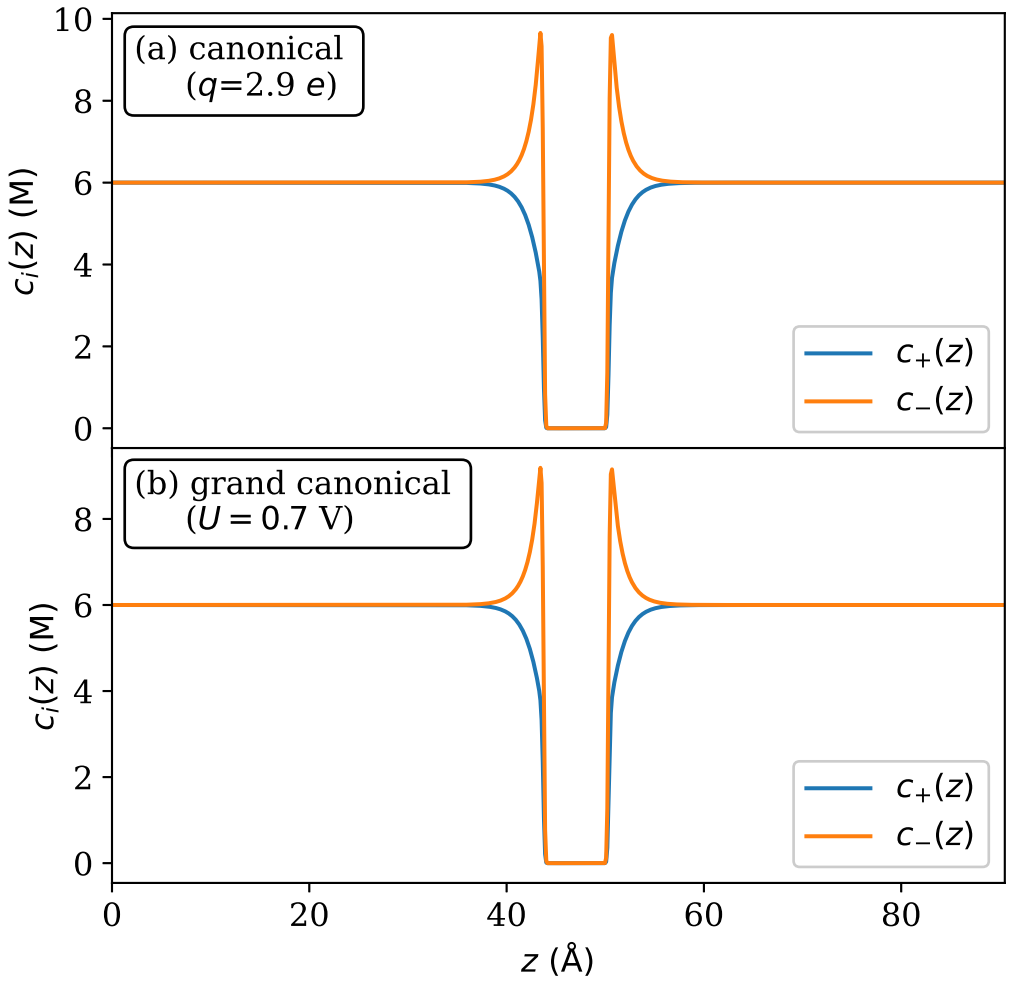

Figure 5: Planar-average concentration profiles of electrolyte ions around a positively charged single layer graphene electrode. (a) Canonical ensemble calculation at $q = 2.9\ e$ (b) Grand canonical ensemble calculation at $U = 0.7$ V.

of linear fits to the data. Our calculated values of electrolyte diffuse layer capacitance for 1-5 layer graphene are shown in the legend which are 12.19 μF/cm^2 , 10.63 μF/cm^2, 11.09 μF/cm^2, 10.88 μF/cm^2 and 10.94 μF/cm^2 respectively. The electrolyte diffuse layer capacitance does not change much with the number of layers of graphene ~~and is quite linear with the potential,~~ as also observed in previous computational studies.[34,36,37] Computational study by Zhan *et al.* reported a value around 13 μF/cm^2 for the electrolyte diffuse layer capacitance in 6 M implicit electrolyte.[37] Experimental values of electrolyte diffuse layer capacitance measured by Ji *et al.* in 6 M KOH, vary around 5-30 μF/cm^2.[31] Gravimetric capacitances reported experimentally at similar electrolyte concentrations vary from 65-150 F/g,[60] 150-205 F/g.[61] Our calculated values translate into gravimetric capacitance of 322 F/g, 140 F/g, 98 F/g, 72 F/g, 58 F/g respectively for 1-5 layer graphene. A larger variation is seen in the values of gravimetric capacitance because of the decrease in gravimetric specific surface area with the number of layers in graphene.

3.1.2 Electrode capacitance due to electronic density of states (C_e)

The excess electronic charge stored per unit area σ_e as a function of the electrode potential U can be calculated from the electronic density of states per unit area $D(\epsilon)$ and the Fermi-Dirac function as:[34,36]

$$\sigma_\mathrm{e}(U) = -e \int D(\epsilon) \left[f_{\mu_\mathrm{e}(U)}(\epsilon) - f_{\mu_\mathrm{e}(U=0)}(\epsilon) \right] d\epsilon, \tag{40}$$

where $f_{\mu_\mathrm{e}(U)}$ is the Fermi-Dirac function (eq. 22) evaluated at the chemical potential $\mu_\mathrm{e}(U) = \mu_\mathrm{e} - e \cdot U$. Here the assumption is that the density of states (DOS) remains the same after applying a potential U. This fixed band assumption is justified as the DOS of graphene does not change much with electrode charging and gives a reasonable estimate of the quantum capacitance which has also been used in several previous studies.[28,34,36,62] A more recent study by Radin *et al.* has computed the quantum capacitance without the fixed-band assumption.[35] To calculate the electronic charge σ_e, the DOS should be very well converged with respect to the surface area of graphene. We thus increase the area of graphene sheets by 4×4

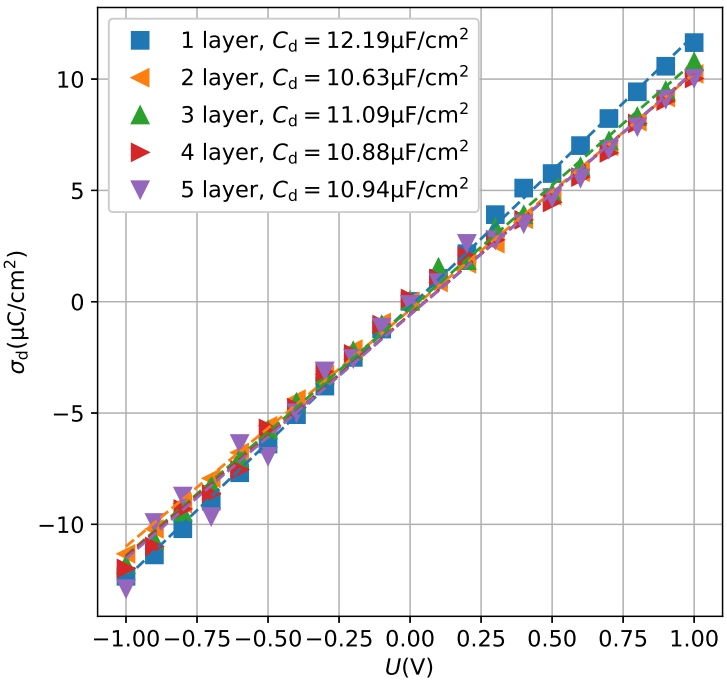

Figure 6: Charge density σ_d versus the electrode potential U for multi-layer graphene in the grand canonical ensemble for electrons. The differential capacitance of the electrolyte diffuse layer C_d is calculated as the slope of linear fits to the data.

times, that is with 1536 atoms in each layer. We calculate the DOS for neutral 1-5 layer graphene in the same electrolyte environment using the canonical approach and obtain the electronic charge-potential curves from eq. (40) which are shown in Fig. 7(a). The derivative of electronic charge σ_e with respect to the electrode potential U is the electronic capacitance C_e, which is shown in Fig. 7(b). The predicted electronic capacitance of a single layer graphene agrees well with the experimentally measured values.[29,30] It can be seen that the electronic capacitance increases with the number of layers of graphene due to the increase in DOS, as also found by previous computational studies.[35–39]

3.1.3 Total capacitance

The total capacitance of multi-layer graphene can be calculated as electrolyte diffuse layer capacitance in series with an electronic capacitance following eq. (37). With the electrolyte diffuse layer capacitance calculated in Sec. 3.1.1 and the electronic capacitance calculated in Sec. 3.1.2, the calculated total capacitance for multi-layer graphene as a function of the electrode potential U is shown in Fig. 8. The total capacitance increases with the number of layers of graphene and soon approaches convergence as also observed in previous computational studies.[35–39] ~~The computed values of total capacitance at $U = -0.2$ V are compared in Fig. 8(b) with the values reported by Radin *et al.*[35] and show good agreement.~~ Experimental study by Ji *et al.* on multilayer graphene in aqueous 6 M KOH electrolyte has reported total capacitance in range of 2-10 µF/cm^2.[31]

3.2 Calibration of absolute electrode potentials

To make our model more useful for performing realistic simulations at constant potentials against experimental reference electrodes, we now calculate the reference chemical potential μ_e^{ref} for the standard hydrogen electrode (SHE) $\mu_e^{SHE} \equiv \mu_e^{H^+/H_2}$ and the Li metal electrode

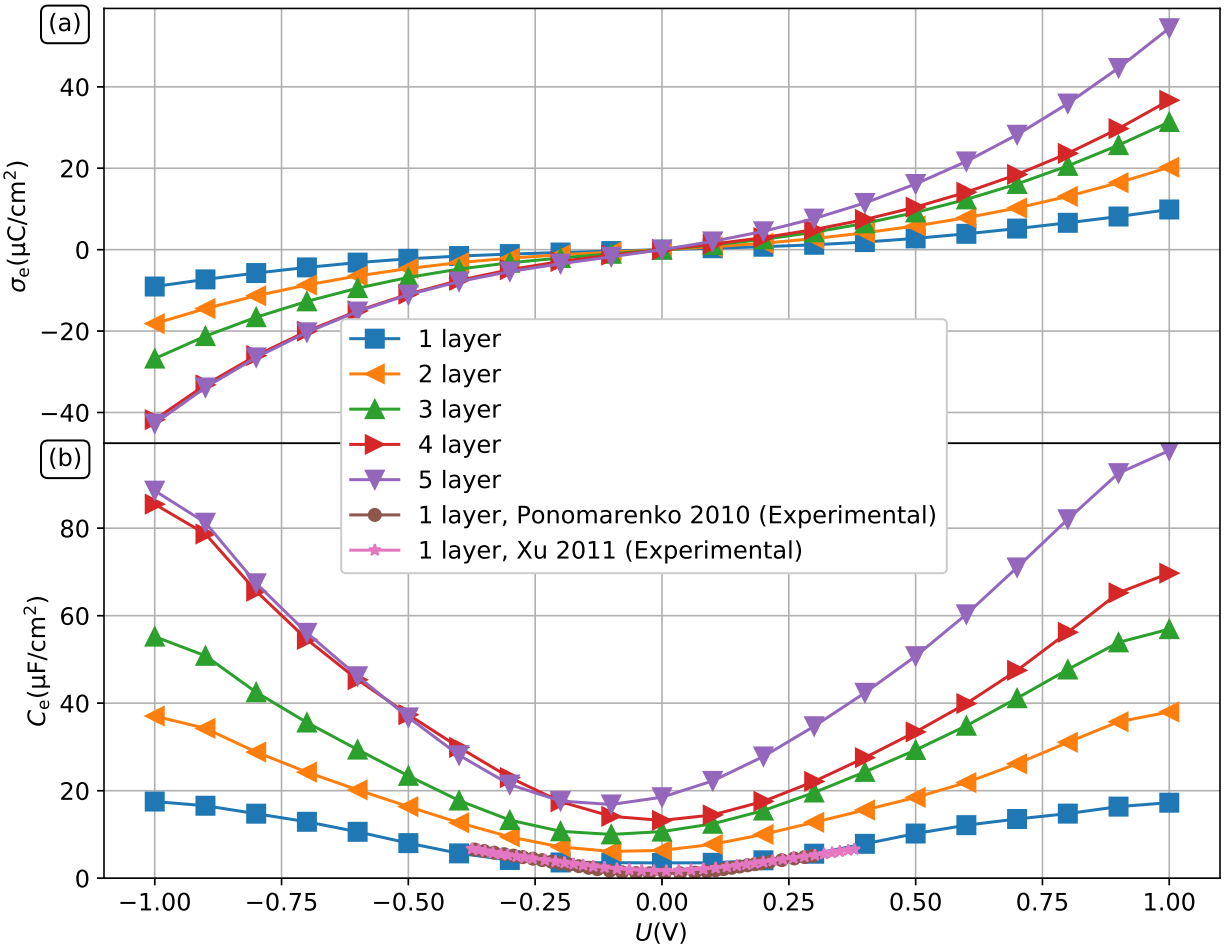

Figure 7: (a) Electronic charge density σ_e (b) Electronic capacitance C_e due to the electronic density of states (DOS) for multi-layer graphene.

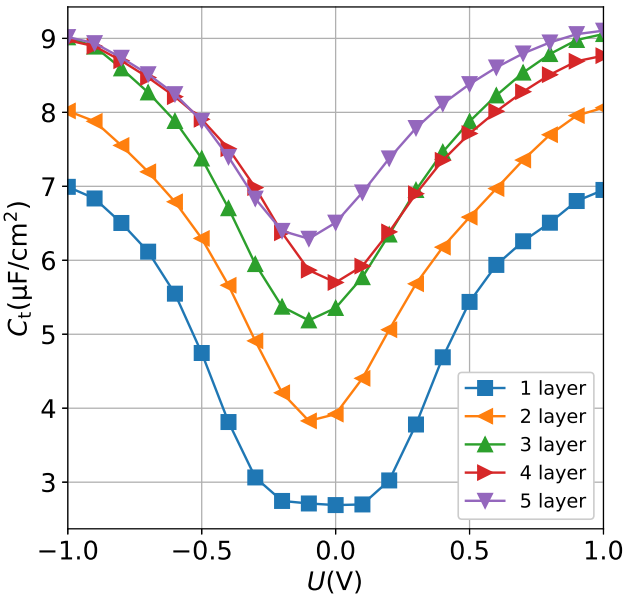

Figure 8: Total capacitance for multi-layer graphene ~~(a)~~ as a function of electrode potential U~~, (b) as a function of the number of layers at $U = -0.2$ V (at the dashed vertical line in (a))~~.

$\mu_e^{\mathrm{Li^+/Li}}$. Following Trasatti,[58] the reduction potential for the SHE can be written as:

$$\mathrm{H^+(aq.)} + e^-(\mathrm{vac.}) \rightarrow 1/2 \cdot \mathrm{H_2(g)} \tag{41}$$

$$\mathcal{E}^{\mathrm{SHE}} = -\Delta G/F = \left[G_{\mathrm{H^+(aq.)}} - 1/2 \cdot G_{\mathrm{H_2(g)}}\right]/F \tag{42}$$

where F is the Faraday constant. Trasatti calculated the reduction potential by breaking eq. (42) into three reactions following a Born-Haber cycle.

$$\mathcal{E}^{\mathrm{SHE}} = \left[\left(G_{\mathrm{H^+(aq.)}} - G_{\mathrm{H^+(vac.)}}\right) + \left(G_{\mathrm{H^+(vac.)}} - G_{\mathrm{H(vac.)}}\right) + \left(G_{\mathrm{H(vac.)}} - 1/2 \cdot G_{\mathrm{H_2(g)}}\right)\right]/F \tag{43}$$

$$= \left[\Delta G_{\mathrm{solvation,H^+}} + \Delta G_{\mathrm{ionization,H}} + \Delta G_{\mathrm{atomization,1/2\cdot H_2}}\right]/F \tag{44}$$

From experimental values of the solvation free energy of $\mathrm{H^+}$, ionization energy of H and atomization energy of $1/2{\cdot}\mathrm{H_2}$, an experimental estimate of $\mathcal{E}^{\mathrm{SHE}}_{\mathrm{exp}} = 4.44$ V has been reached.[58] Now from our model we aim to calculate the reduction potential $\mathcal{E}$ directly from eq. (42).

From the point of view of DFT- computations, a calculation of H^+ is not possible because it has no electrons. We thus modify the reaction as:

$$H^+ \cdot H_2O(\text{aq.}) + e^-(\text{vac.}) \rightarrow 1/2 \cdot H_2(\text{g}) + H_2O(\text{aq.}) \tag{45}$$

$$\mathcal{E}^{\text{SHE}} = -\Delta G/F = \left[G_{H^+ \cdot H_2O(\text{aq.})} - 1/2 \cdot G_{H_2(\text{g})} - G_{H_2O(\text{aq.})}\right]/F \tag{46}$$

We perform three calculations: of a hydronium ion ($H^+ \cdot H_2O(\text{aq.})$), a hydrogen diatomic molecule ($H_2(\text{g})$) and a water molecule ($H_2O(\text{aq.})$). We include translational, rotational and vibrational free energy corrections for each molecule. We include the free energy correction in the calculation of $H_2(\text{g})$ due to a standard pressure of 1 atm. The aqueous environment is represented as a Poisson-Boltzmann electrolyte of concentration $c_i^\infty = c^\circ$=1 M in an implicit solvent with bulk permittivity of 78.54 and a surface tension of 0.07415 N/m corresponding to that of water at 298.15 K. We use the soft-sphere model for the solvent permittivity function and compute the reduction potential from eq. (46) for several different values of soft-sphere radii as shown in Table 2. The ratio of O radius to H radius is kept the same as the ratio of their van der Waals radii. We see that the soft-sphere radius values of 2.644 a_0 for H and 3.311 a_0 for O give an electrode potential $\mathcal{E}^{\text{SHE}} = 4.45$ V, which is close to the experimental value $\mathcal{E}^{\text{SHE}}_{\text{exp}} = 4.44$ V reported by Trasatti.[58] These values of the soft-sphere radii can be used along with $\mu_{\text{e}}^{\text{SHE}} = -e \cdot \mathcal{E}^{\text{SHE}} = -4.45$ eV to perform simulations at constant potentials with respect to the SHE. Another relevant quantity, the proton work function calculated as $W_{H^+ \cdot H_2O(\text{aq.})} = G_{H_2O(\text{aq.})} - G_{H^+ \cdot H_2O(\text{aq.})}$ is also shown in Table 2. The experimental value is 11.36 eV, as shown in Table 1 of Cheng *et al.*[63] We see that the soft-sphere radius values of 2.599 a_0 for H and 3.254 a_0 for O give a proton work function $W_{H^+ \cdot H_2O(\text{aq.})} = 11.35$ eV, which is close to the experimental value. Further, similar values of soft-sphere radii give a reasonable prediction for both: the absolute electrode potential and the proton work function.

Similarly, we calculate the absolute electrode potential of a Li metal electrode which is

Table 2: The computed absolute electrode potential $\mathcal{E}^{\mathrm{SHE}}$ for a standard hydrogen electrode (SHE) from eq. (46) for several values of soft-sphere radii for the solvent permittivity function. The proton work function $W_{\mathrm{H^+\cdot H_2O(aq.)}}$ is also shown.

H radius (a_0)	O radius (a_0)	$\mathcal{E}^{\mathrm{SHE}}$ (V)	$W_{\mathrm{H^+\cdot H_2O(aq.)}}$ (eV)
3.006	3.764	4.96	10.76
2.825	3.538	4.72	10.99
2.780	3.481	4.62	11.05
2.712	3.396	4.56	11.16
2.644	3.311	4.45	11.27
2.599	3.254	4.37	11.35
2.260	2.830	3.63	12.09

often used as a reference electrode in the Li-ion batteries. The reduction potential for Li metal electrode can be written as:

$$\mathrm{Li^+(solv.)} + e^-(\mathrm{vac.}) \rightarrow \mathrm{Li(s)} + \mathrm{p.e.} \tag{47}$$

$$\mathcal{E}^{\mathrm{Li^+/Li}} = -\Delta G/F = \left[G_{\mathrm{Li^+(solv.)}} - G_{\mathrm{p.e.}} - G_{\mathrm{Li(s)}}\right]/F. \tag{48}$$

For $G_{\mathrm{Li^+(solv.)}}$, we perform a calculation of a single Li-ion in a solvated environment, $G_{\mathrm{p.e.}}$ refers to the energy of the pure electrolyte in the same simulation cell and $G_{\mathrm{Li(s)}}$ is calculated as the energy per Li-atom of a 1024-atom bulk Li solid. We calibrate the soft-sphere radius for Li and the computed reduction potentials are shown in Table 3. We see that a soft-sphere radius of 3.048 a_0 gives an electrode potential $\mathcal{E}^{\mathrm{Li^+/Li}} = 1.40$ V, which is close to the experimental value $\mathcal{E}^{\mathrm{Li^+/Li}}_{\mathrm{exp}} = 1.39$ V.[58] We recommend using the calibrated soft-sphere radius along with setting $\mu_{\mathrm{e}}^{\mathrm{Li^+/Li}} = -e \cdot \mathcal{E}^{\mathrm{Li^+/Li}} = -1.40$ eV for performing simulations relevant for the Li-ion batteries with Li metal electrode as the reference electrode.

After calibrating the soft-sphere radii which give a reasonable prediction of the reduction potential of Li in aqueous electrolyte, we investigate the charging behaviour of graphene on connecting to this Li metal electrode. We use an aqueous electrolyte solution for this application and the same scaled soft-sphere radii parameters as obtained from the calibration of reduction potential of Li. This can be seen as a preliminary application of our model

Table 3: The computed absolute electrode potential $\mathcal{E}^{\mathrm{Li^+/Li}}$ for Li metal electrode from eq. (48) for several values of soft-sphere radii for solvent permittivity function.

Li radius (a_0)	$\mathcal{E}^{\mathrm{Li^+/Li}}$ (V)
3.208	1.81
3.128	1.61
3.088	1.51
3.048	1.40
3.007	1.30
2.967	1.18

similar to experiments on initial Li-ion batteries that were done in aqueous electrolyte.[64,65] While modern Li-ion batteries use multiple electrolyte salts in various mixtures of organic solvents, we defer these complicated systems for future studies.

3.3 ~~Demonstration of model in~~ Towards modelling of Li-ion batteries

During ultra short current spikes in a Li-ion battery, while the normal intercalation process is limited by slow ion diffusion and charge transfer resistance, the fast interfacial charge storage at the surfaces of the electrode nanoparticles provides additional power density while suppressing excessive overpotentials. We demonstrate an exemplar application on the interfacial charge developed on a 5-layer graphene slab in a Li-ion battery. We compare the cases of a canonical (constant charge) simulation ($q = 0.0\ e$) with the newly-developed grand canonical (constant voltage) method. In Fig. 9 we show the planar-average electrolyte concentration profiles around the graphene slab. In the canonical calculation shown in Fig. 9(a), the total charge is zero on the graphene slab which does not polarize the electrolyte, thereby producing the same profiles for negative and positive electrolyte reaching asymptotically the bulk value $c_i^\infty = 6$ M. In Fig. 9(b) we use the grand canonical scheme and couple the graphene anode to the $\mathrm{Li^+/Li}$ reference electrode, thereby setting the electrochemical potential of electrons as $\tilde{\mu}_\mathrm{e} = \mu_\mathrm{e} = \mu_\mathrm{e}^{\mathrm{Li^+/Li}} = -1.40$ eV. This gives a total charge of $-6.7\ e$ on the graphene slab leading to an increase in the concentration of positive electrolyte around the graphene slab

and a depletion of the concentration of the negative electrolyte around the graphene slab, showing the formation of electrolyte double layers. In Fig. 9(c), we further add a potential of $U = 1.0$ V with respect to Li^+/Li, thereby setting the electrochemical potential of electrons as $\tilde{\mu}_e = \mu_e = \mu_e^{Li^+/Li} - e \cdot U = -2.40$ eV. This gives a total charge of -3.5 e on the graphene slab. This is in agreement with the fact that a reduction in the Fermi level would decrease the number of electrons in the system. Correspondingly, the peaks of positive electrolyte around the graphene slab are lowered in (c) as compared to case (b) due to the reduction of the number of electrons and therefore, a lower number of positive electrolyte ions needed for achieving electroneutrality.

The change in charge densities in the system at $U = 1.0$ V (with respect to Li^+/Li) from the system at $U = 0.0$ V (with respect to Li^+/Li) is shown in Fig. 10. In Fig. 10(a) we show the difference in electrolyte density in a plane cutting the 5-layer graphene orthogonally. We see that more positive electrolyte density is accumulated near the surface for a system at $U = 0.0$ V as compared to the system at $U = 1.0$ V. This is because of a higher number of electrons in a system at $U = 0.0$ V (6.7 electrons) as compared to the system at $U = 1.0$ V (3.5 electrons) thus, more positive electrolyte is needed to achieve electroneutrality.

The corresponding difference in the electronic density is shown in Fig. 10(b). Two isosurfaces of electronic density are drawn at $\rho_e(\mathbf{r}) = \pm 2.0 \times 10^{-3}$ $e/\text{Å}^3$. Blue color shows a gain of electronic density, while the red color shows a depletion in electronic density. The extra electronic charge density in a system at $U = 0.0$ V is predominantly localized at the surface and decreases in the subsurface graphene layers. The difference in charges on different layers as obtained from Mulliken population analysis is -2.8 e on the outermost surface layers, -0.3 e on subsurface layers and -0.1 e on the central layer totalling a charge difference of -3.2 e (in other words, a gain of 3.2 electrons in the system at $U = 0.0$ V as compared to the system at $U = 1.0$ V). Thus the electrons and electrolyte mutually affect each other upon a variation in the voltage, similar to an experimental setup.

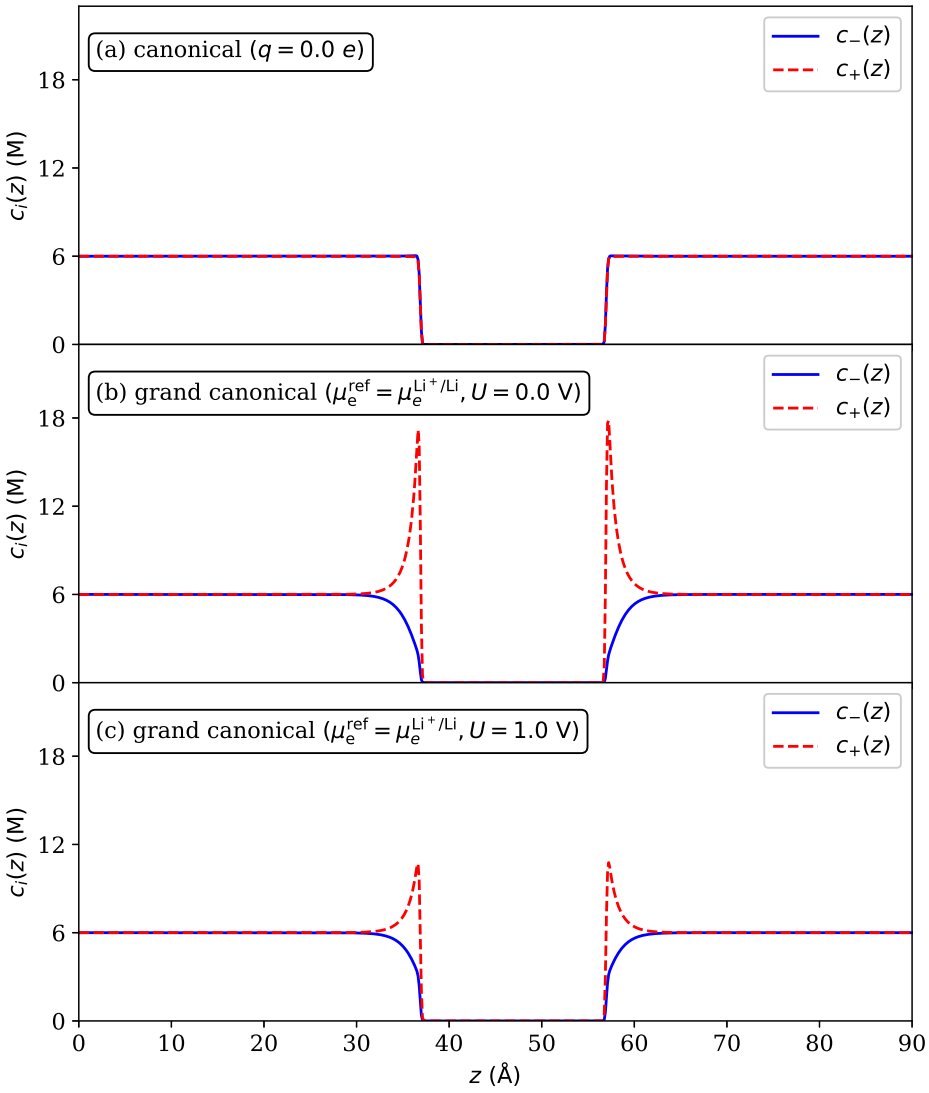

Figure 9: Electrolyte concentration around a 5-layer graphene slab. (a) Canonical calculation at constant charge ($q = 0.0\ e$), (b) grand canonical calculation with Li^+/Li as the reference electrode at $U = 0.0$ V (c) same as (b) but at $U = 1.0$ V

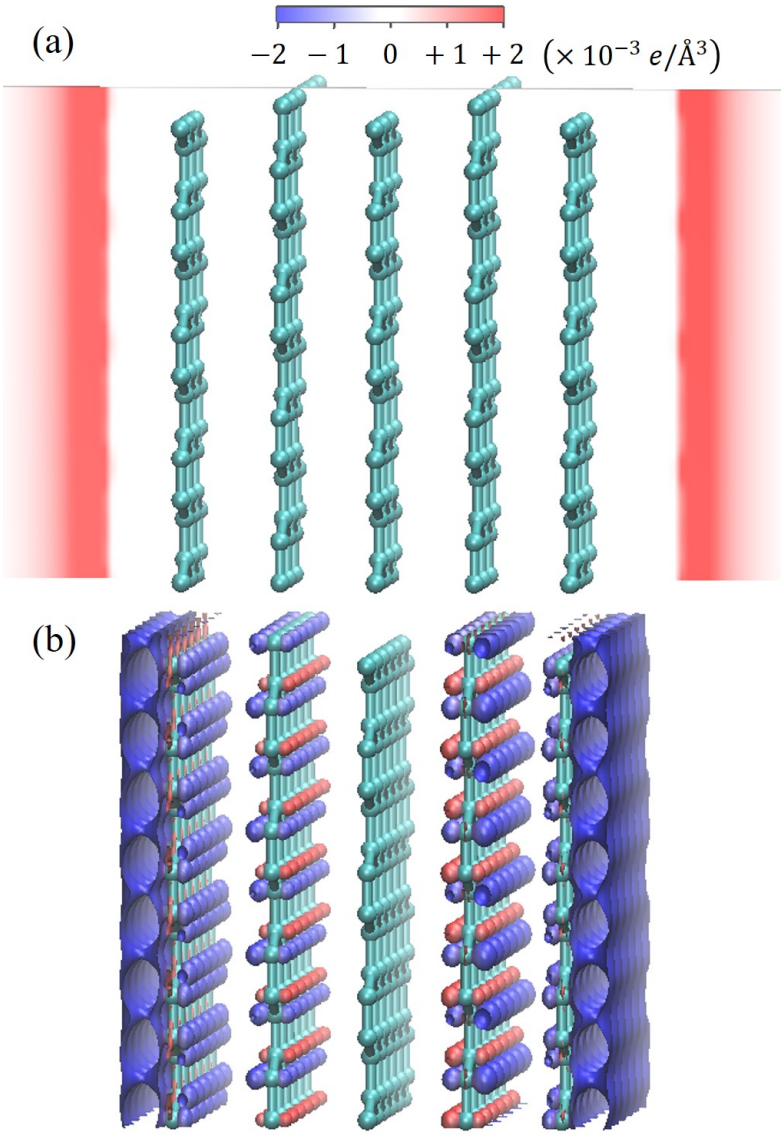

Figure 10: Difference in charge densities of a system at $U = 1.0$ V (with respect to Li^+/Li) from a system at $U = 0.0$ V (with respect to Li^+/Li). (a) Electrolyte density ρ_d in a plane bisecting the 5-layer graphene sheet orthogonally, (b) Electronic density isosurfaces at $\rho_e(\mathbf{r}) = \pm 2.0 \times 10^{-3}\ e/Å^3$.

4 Conclusions

We have developed a powerful and elegant new hybrid computational method combining Density Functional Theory (DFT) and the Poisson-Boltzmann equation (P-BE) which is capable of simulating experimental electrochemistry, in the presence of solvent and electrolyte. The method has been implemented in a way that offers several major advantages: Firstly, it allows the simulations to take place under potential control, as in experimental electrochemistry. Secondly, it is based on linear-scaling DFT which can model nanoscale systems with thousands of atoms allowing all complex materials features of the charged electrode to be represented quantum-mechanically while neutralized by a counter electrolyte charge. Finally, our approach can be calibrated with respect to common reference electrodes such as the standard hydrogen electrode and the Li-metal electrode, which is used as a reference electrode in Li-ion batteries.

We have demonstrated exemplar applications on the differential capacitance of graphene based electrodes in supercapacitors and interfacial charge developed while connecting a graphene based electrode with a Li metal electrode in a battery. However, our newly-developed grand canonical method for performing simulations at constant voltage in electrolyte environment, within linear-scaling DFT, is a general computational method for *ab initio* electrochemistry and can be applied to all kinds of situations related to charged electrochemical interfaces.

The electrolyte model in ONETEP is under active development. There are several assumptions of the current model, which can be improved in further developments. One of these is a linear dielectric response of the solvent. The model can be extended to include non-linear response of the solvent which has been found to be important in applications in Li-ion batteries.[41] Another assumption is the point-size of electrolyte ions. The model can be extended to include finite-size steric effects of electrolyte ions[66] which can have significant effect on the differential capacitance.[15] The solvated electrolyte ions in Li-ion batteries have finite steric size. Hence, these effects can be significant in such applications. The

model together with further developments will lead to a platform for large-scale atomistic simulations in electrochemistry from first principles. It can be used to produce predictions that use the same language as experimentalists, enabling a new frontier in materials science: computational electrochemical interface design.

5 Acknowledgements

This work was carried out with funding from the Faraday Institution (faraday.ac.uk; EP/S003053/1), grant number FIRG003. The majority of computations presented in this work were performed on the Iridis5 supercomputer of the University of Southampton and the Michael supercomputer of the Faraday Institution. We acknowledge the United Kingdom Materials and Molecular Modelling Hub for computational resources, partially funded by EPSRC (EP/P020194/1).

Data availability

The data that supports the findings of this study is available within the article.

References

(1) Schmickler, W.; Santos, E. *Interfacial electrochemistry*, 2nd ed.; Springer-Verlag Berlin Heidelberg, 2010; pp 1–272.

(2) Bard, A. J.; Faulkner Larry R., *Electrochemical Methods: Fundamentals and Applications*, 2nd ed.; John Wiley Sons, Ltd, 2010; pp 1–864.

(3) Swift, M. W.; Swift, J. W.; Qi, Y. Modeling the electrical double layer at solid-state electrochemical interfaces. *Nature Computational Science* **2021**, *1*, 212–220.

(4) Jones, R. O. Density functional theory: Its origins, rise to prominence, and future. *Reviews of Modern Physics* **2015**, *87*, 897–923.

(5) Kohn, W.; Becke, A. D.; Parr, R. G. Density Functional Theory of Electronic Structure. *The Journal of Physical Chemistry* **1996**, *100*, 12974–12980.

(6) Wang, A.; Kadam, S.; Li, H.; Shi, S.; Qi, Y. Review on modeling of the anode solid electrolyte interphase (SEI) for lithium-ion batteries. *NPJ Computational Materials* **2018**, *4*.

(7) Kang, J.; Wei, S. H.; Zhu, K.; Kim, Y. H. First-principles theory of electrochemical capacitance of nanostructured materials: Dipole-assisted subsurface intercalation of lithium in pseudocapacitive TiO2 anatase nanosheets. *The Journal of Physical Chemistry C* **2011**, *115*, 4909–4915.

(8) Jorn, R.; Kumar, R.; Abraham, D. P.; Voth, G. A. Atomistic modeling of the electrode-electrolyte interface in Li-ion energy storage systems: Electrolyte structuring. *The Journal of Physical Chemistry C* **2013**, *117*, 3747–3761.

(9) Skyner, R. E.; McDonagh, J. L.; Groom, C. R.; Van Mourik, T.; Mitchell, J. B. A review of methods for the calculation of solution free energies and the modelling of systems in solution. *Physical Chemistry Chemical Physics* **2015**, *17*, 6174–6191.

(10) Hansen, M. H.; Rossmeisl, J. PH in Grand Canonical Statistics of an Electrochemical Interface. *The Journal of Physical Chemistry C* **2016**, *120*, 29135–29143.

(11) Dufils, T.; Jeanmairet, G.; Rotenberg, B.; Sprik, M.; Salanne, M. Simulating Electrochemical Systems by Combining the Finite Field Method with a Constant Potential Electrode. *Physical Review Letters* **2019**, *123*, 195501.

(12) Zhang, C.; Sayer, T.; Hutter, J.; Sprik, M. Modelling electrochemical systems with finite field molecular dynamics. *Journal of Physics: Energy* **2020**, 0–21.

(13) Cramer, C. J.; Truhlar, D. G. Implicit Solvation Models: Equilibria, Structure, Spectra, and Dynamics. *Chemical Reviews* **1999**, *99*, 2161–2200.

(14) Tomasi, J.; Mennucci, B.; Cammi, R. Quantum mechanical continuum solvation models. *Chemical Reviews* **2005**, *105*, 2999–3093.

(15) Nattino, F.; Truscott, M.; Marzari, N.; Andreussi, O. Continuum models of the electrochemical diffuse layer in electronic-structure calculations. *The Journal of Chemical Physics* **2019**, *150*, 41722.

(16) Dziedzic, J.; Bhandari, A.; Anton, L.; Peng, C.; Womack, J. C.; Famili, M.; Kramer, D.; Skylaris, C.-K. A Practical Approach to Large Scale Electronic Structure Calculations in Electrolyte Solutions via Continuum-Embedded Linear-Scaling DFT. *The Journal of Physical Chemistry C* **2020**, *124*, 7860–7872.

(17) Bhandari, A.; Anton, L.; Dziedzic, J.; Peng, C.; Kramer, D.; Skylaris, C.-K. Electronic structure calculations in electrolyte solutions: Methods for neutralization of extended charged interfaces. *The Journal of Chemical Physics* **2020**, *153*, 124101.

(18) Kohn, W.; Sham, L. J. Self-Consistent Equations Including Exchange and Correlation Effects. *Physical Review* **1965**, *140*, A1133–A1138.

(19) Parr, R. G.; Yang, W. Density functional theory of atoms and molecules. *Oxford University Press* **1989**, *1*, 989.

(20) Sundararaman, R.; Goddard, W. A.; Arias, T. A. Grand canonical electronic density-functional theory: Algorithms and applications to electrochemistry. *The Journal of Chemical Physics* **2017**, *146*.

(21) Melander, M. M.; Kuisma, M. J.; Christensen, T. E. K.; Honkala, K. Grand-canonical approach to density functional theory of electrocatalytic systems: Thermodynamics of

solid-liquid interfaces at constant ion and electrode potentials. *The Journal of Chemical Physics* **2019**, *150*.

(22) Hörmann, N. G.; Andreussi, O.; Marzari, N. Grand canonical simulations of electrochemical interfaces in implicit solvation models. *The Journal of Chemical Physics* **2019**, *150*.

(23) Prentice, J. C. A. et al. The ONETEP linear-scaling density functional theory program. *The Journal of Chemical Physics* **2020**, *152*, 174111.

(24) Dziedzic, J.; Helal, H. H.; Skylaris, C. K.; Mostofi, A. A.; Payne, M. C. Minimal parameter implicit solvent model for ab initio electronic-structure calculations. *Europhysics Letters* **2011**, *95*, 1–6.

(25) Dziedzic, J.; Fox, S. J.; Fox, T.; Tautermann, C. S.; Skylaris, C. K. Large-scale DFT calculations in implicit solvent - A case study on the T4 lysozyme L99A/M102Q protein. *International Journal of Quantum Chemistry* **2013**, *113*, 771–785.

(26) Pumera, M. Graphene-based nanomaterials for energy storage. *Energy and Environmental Science* **2011**, *4*, 668–674.

(27) Xu, C.; Xu, B.; Gu, Y.; Xiong, Z.; Sun, J.; Zhao, X. S. Graphene-based electrodes for electrochemical energy storage. *Energy and Environmental Science* **2013**, *6*, 1388–1414.

(28) Xia, J.; Chen, F.; Li, J.; Tao, N. Measurement of the quantum capacitance of graphene. *Nature Nanotechnology* **2009**, *4*, 505–509.

(29) Ponomarenko, L. A.; Yang, R.; Gorbachev, R. V.; Blake, P.; Mayorov, A. S.; Novoselov, K. S.; Katsnelson, M. I.; Geim, A. K. Density of states and zero Landau level probed through capacitance of graphene. *Physical Review Letters* **2010**, *105*, 1–4.

(30) Xu, H.; Zhang, Z.; Peng, L. M. Measurements and microscopic model of quantum capacitance in graphene. *Applied Physics Letters* **2011**, *98*.

(31) Ji, H.; Zhao, X.; Qiao, Z.; Jung, J.; Zhu, Y.; Lu, Y.; Zhang, L. L.; MacDonald, A. H.; Ruoff, R. S. Capacitance of carbon-based electrical double-layer capacitors. *Nature Communications* **2014**, *5*.

(32) Downard, A. J.; Farquhar, A. K.; Brooksby, P. A. Measuring the Capacitance at Few- and Many-Layered Graphene Electrodes in Aqueous Acidic Solutions. *The Journal of Physical Chemistry C* **2018**, *122*, 6103–6108.

(33) Farquhar, A. K.; Brooksby, P. A.; Downard, A. J. Controlled Spacing of Few-Layer Graphene Sheets Using Molecular Spacers: Capacitance That Scales with Sheet Number. *ACS Applied Nano Materials* **2018**, *1*, 1420–1429.

(34) Paek, E.; Pak, A. J.; Hwang, G. S. A Computational Study of the Interfacial Structure and Capacitance of Graphene in [BMIM][PF 6] Ionic Liquid . *Journal of The Electrochemical Society* **2013**, *160*, A1–A10.

(35) Radin, M. D.; Ogitsu, T.; Biener, J.; Otani, M.; Wood, B. C. Capacitive charge storage at an electrified interface investigated via direct first-principles simulations. *Physical Review B* **2015**, *91*, 1–7.

(36) Zhan, C.; Neal, J.; Wu, J.; Jiang, D.-E. Quantum Effects on the Capacitance of Graphene-Based Electrodes. *The Journal of Physical Chemistry C* **2015**, *119*, 22297–22303.

(37) Zhan, C.; Jiang, D.-E. Contribution of Dielectric Screening to the Total Capacitance of Few-Layer Graphene Electrodes. *Journal of Physical Chemistry Letters* **2016**, *7*, 789–794.

(38) Zhan, C.; Zhang, Y.; Cummings, P. T.; Jiang, D.-E. Computational insight into the capacitive performance of graphene edge planes. *Carbon* **2017**, *116*, 278–285.

(39) Lian, C.; Zhan, C.; Jiang, D.-E.; Liu, H.; Wu, J. Capacitive Energy Extraction by Few-Layer Graphene Electrodes. *The Journal of Physical Chemistry C* **2017**, *121*, 14010–14018.

(40) Letchworth-Weaver, K.; Arias, T. A. Joint density functional theory of the electrode-electrolyte interface: Application to fixed electrode potentials, interfacial capacitances, and potentials of zero charge. *Physical Review B* **2012**, *86*, 1–16.

(41) Gunceler, D.; Letchworth-Weaver, K.; Sundararaman, R.; Schwarz, K. A.; Arias, T. A. The importance of nonlinear fluid response in joint density-functional theory studies of battery systems. *Modelling and Simulation in Materials Science and Engineering* **2013**, *21*.

(42) Mathew, K.; Kolluru, V. S.; Mula, S.; Steinmann, S. N.; Hennig, R. G. Implicit self-consistent electrolyte model in plane-wave density-functional theory. *The Journal of Chemical Physics* **2019**, *151*.

(43) Raccichini, R.; Amores, M.; Hinds, G. Critical Review of the Use of Reference Electrodes in Li-Ion Batteries: A Diagnostic Perspective. *Batteries* **2019**, *5*.

(44) Franco, A. A. Multiscale modelling and numerical simulation of rechargeable lithium ion batteries: Concepts, methods and challenges. *RSC Advances* **2013**, *3*, 13027–13058.

(45) Grochowski, P.; Trylska, J. Continuum molecular electrostatics, salt effects, and counterion binding – A review of the Poisson-Boltzmann theory and its modifications. *Biopolymers* **2008**, *89*, 93–113.

(46) Gray, C. G.; Stiles, P. J. Nonlinear electrostatics: the Poisson–Boltzmann equation. *European Journal of Physics* **2018**, *39*, 053002.

(47) Fattebert, J. L.; Gygi, F. Density functional theory for efficient ab initio molecular

dynamics simulations in solution. *Journal of Computational Chemistry* **2002**, *23*, 662–666.

(48) Fisicaro, G.; Genovese, L.; Andreussi, O.; Mandal, S.; Nair, N. N.; Marzari, N.; Goedecker, S. Soft-Sphere Continuum Solvation in Electronic-Structure Calculations. *Journal of Chemical Theory and Computation* **2017**, *13*, 3829–3845.

(49) Bramley, G.; Nguyen, M. T.; Glezakou, V. A.; Rousseau, R.; Skylaris, C. K. Reconciling Work Functions and Adsorption Enthalpies for Implicit Solvent Models: A Pt (111)/Water Interface Case Study. *Journal of Chemical Theory and Computation* **2020**, *16*, 2703–2715.

(50) Womack, J. C.; Anton, L.; Dziedzic, J.; Hasnip, P. J.; Probert, M. I.; Skylaris, C. K. DL_MG: A Parallel Multigrid Poisson and Poisson-Boltzmann Solver for Electronic Structure Calculations in Vacuum and Solution. *Journal of Chemical Theory and Computation* **2018**, *14*, 1412–1432.

(51) *http://www.dlmg.org*

(52) Goedecker, S. Linear scaling electronic structure methods. *Reviews of Modern Physics* **1999**, *71*, 1085–1123.

(53) Skylaris, C. K.; Haynes, P. D.; Mostofi, A. A.; Payne, M. C. Introducing ONETEP: Linear-scaling density functional simulations on parallel computers. *The Journal of Chemical Physics* **2005**, *122*, 1–10.

(54) Skylaris, C.-K.; Mostofi, A. A.; Haynes, P. D.; Diéguez, O.; Payne, M. C. Nonorthogonal generalized Wannier function pseudopotential plane-wave method. *Physical Review B* **2002**, *66*, 035119.

(55) Mostofi, A. A.; Haynes, P. D.; Skylaris, C.-K.; Payne, M. C. Preconditioned iterative

minimization for linear-scaling electronic structure calculations. *The Journal of Chemical Physics* **2003**, *119*, 8842–8848.

(56) Ruiz-Serrano, Á.; Skylaris, C.-K. A variational method for density functional theory calculations on metallic systems with thousands of atoms. *The Journal of Chemical Physics* **2013**, *139*, 054107.

(57) Kerker, G. P. Efficient iteration scheme for self-consistent pseudopotential calculations. *Physical Review B* **1981**, *23*, 3082–3084.

(58) Trasatti, S. The absolute electrode potential: an explanatory note (Recommendations 1986). *Pure and Applied Chemistry* **1986**, *58*, 955 – 966.

(59) Ohshima, H.; Matsubara, H. Surface tension of electrolyte solutions. *Colloid and Polymer Science* **2004**, *282*, 1044–1048.

(60) Du, X.; Guo, P.; Song, H.; Chen, X. Graphene nanosheets as electrode material for electric double-layer capacitors. *Electrochimica Acta* **2010**, *55*, 4812–4819.

(61) Li, H. Q.; Wang, Y. G.; Wang, C. X.; Xia, Y. Y. A competitive candidate material for aqueous supercapacitors: High surface-area graphite. *Journal of Power Sources* **2008**, *185*, 1557–1562.

(62) Stoller, M. D.; Magnuson, C. W.; Zhu, Y.; Murali, S.; Suk, J. W.; Piner, R.; Ruoff, R. S. Interfacial capacitance of single layer graphene. *Energy and Environmental Science* **2011**, *4*, 4685–4689.

(63) Cheng, J.; Sprik, M. Alignment of electronic energy levels at electrochemical interfaces. *Physical Chemistry Chemical Physics* **2012**, *14*, 11245–11267.

(64) Li, W.; Dahn, J. R.; Wainwright, D. S. Rechargeable Lithium Batteries with Aqueous Electrolytes. *Science* **1994**, *264*, 1115–1118.

(65) Reiman, K. H.; Brace, K. M.; Gordon-Smith, T. J.; Nandhakumar, I.; Attard, G. S.; Owen, J. R. Lithium insertion into TiO2 from aqueous solution - Facilitated by nanostructure. *Electrochemistry Communications* **2006**, *8*, 517–522.

(66) Borukhov, I.; Andelman, D.; Orland, H. Steric Effects in Electrolytes: A Modified Poisson-Boltzmann Equation. *Physical Review Letters* **1997**, *79*, 435–438.